Density Functional Theory Investigation of Product Distribution following Reaction of Acrylonitrile on Diamond (001)-2×1 Surface

Laibin Zhang,[†] Tingqi Ren,[†] Hongming Wang,*[,‡] Meishan Wang,*[,†,§] Chuanlu Yang,[†] and Keli Han[†,§]

School of Physics and Electronic Engineering, Key Laboratory of Atomic and Molecular Physics of Shandong Province, Ludong University, Yantai, 264025, China, Department of Chemistry, Zhengzhou University, Zhengzhou, 450001, China, and State Key Laboratory of Molecular Reaction Dynamics, Dalian Institute of Chemical Physics, Dalian, 116023, China

Received: June 14, 2006; In Final Form: September 18, 2006

The reaction of acrylonitrile with the C(001)-2×1 surface has been investigated by employing density functional cluster model calculations. The calculations revealed eight possible reaction pathways for acrylonitrile with the surface dimer. Full geometry optimized structures were obtained for all adducts, including intra- and interdimer reaction products. These results were analyzed in terms of both the total energy values and the detailed optimized geometries. We find that the reaction of acrylonitrile with the diamond (001) surface occurs primarily through its nonpolar C═C group and the intradimer $[2+2]_{cc}$ product is the dominant product. All these results are in good agreement with the experimental work by Schwartz. It is noteworthy that the isomerization process plays an important role in the chemisorption process. Both intradimer [4+2] product and interdimer $[2+2]_{cc}$ product can isomerize to the intradimer $[2+2]_{cc}$ product. The present study shows that the isomerization between intradimer [4+2] product and intradimer $[2+2]_{cc}$ product is slightly favorable over the direct path to formation of the intradimer $[2+2]_{cc}$ product.

1. Introduction

The fascinating and unique combination of mechanical, electrical, thermal, and optical properties of diamond makes it one of the most promising candidates for a wide variety of applications.[1−4] For example, diamond with its (indirect) band gap of 5.5 eV is in fact an extreme electronic material in almost all respects. The organic and biological functionalization of diamond surface can be potentially useful to tailor its properties for specific applications.[5−12] For instance, it was found that incorporation of nitrogen into the diamond lattice affects its thermal conductivity, optical transparency, band gap, and hardness.[3,11−12] Consequently, it is meaningful to investigate the chemical modification of diamond.

Surface reactions of unsaturated organic compounds with the diamond (001)-2×1 reconstructed surface have been good examples for both theory and experiment. Indeed, recently, great effort has been devoted to understanding how organic molecules react with the surfaces of diamond.[13−22] For instance, experimentally, Hovis et al.[13] carefully investigated the nature of [2+2] cycloaddition reaction on C, Si, and Ge surfaces, they predicted that cycloaddition reactions analogous to those observed previously on Si and Ge surfaces also take place on diamond surfaces; the lower reaction probability on diamond (001) is likely associated with its larger band gap and the absence of dimer tilting.[13] Theoretically, it was predicted that 1,3-dipolar cycloadditions of a series of 1,3-dipolar molecules onto the C(100) surface are much more favorable over their molecular analogues both thermodynamically and kinetically.[14,15] Similarly, Long et al.[16] studied the hydroboration of three allotropes of carbon with borane, they predicted that the hydroboration of C(001)-2×1 occurs readily and the as-hydroborated carbonous materials can be good starting points for further chemical modification and manipulation. Recently, Xu's group[18,19] reported several new achievements in the chemical modification and functionalization of diamond. They found that the well-known cycloaddition reactions of carbenes and nitrenes to alkenes in organic chemistry can be employed as a new type of surface reaction to organically functionalize the X(100) surfaces (X = C, Si or Ge) at low temperature. They also predicted the viability of epoxidation of the C(100) surface by organic dioxiranes; those results are interesting and provide a new alternative for oxidation of the diamond (100) surface.[20] Most recently, by means of effective cluster models calculations, they studied the cycloadditions of various substituted carbenes, silylenes, and germylenes onto the C(100) surface, their results reveal that the substituents do play an important effect on the reaction energetics and the detailed reaction pathways.[21] More fascinating is the experimental work reported by Schwartz et al.[22] that acrylonitrile chemisorbed on diamond and silicon (001)-2×1 surfaces at room temperature yield very different product distributions: while the acrylonitrile reacts with C(001) surface largely via the vinyl group, reaction with the Si(001) surface largely through the nitrile group. These findings are quite encouraging and significant because they strongly demonstrate the feasibility of functionalizing diamond surfaces by means of synthetic organic chemistry, which may consequently lead to a breakthrough in the fabrication of diamond films at low temperature.

It is well-known that the C(001) surface exhibits a 2×1 reconstruction in which surface atoms with unsaturated valences pair up to form dimers.[23−25] The bond between the dimer atoms is essentially a strained double bond, with σ and π components. This suggests that the surface may react toward small organic molecules very much like a molecular carbon−carbon double bond. In this work, we have investigated the adsorption of acrylonitrile on diamond (001)-2×1 surface using density

* Corresponding authors: e-mail hmwang@dicp.ac.cn (H.W.) or mswang1971@163.com (M.W.).
[†] Ludong University.
[‡] Zhengzhou University.
[§] Dalian Institute of Chemical Physics.

10.1021/jp063714q CCC: $33.50
Published on Web 10/24/2006

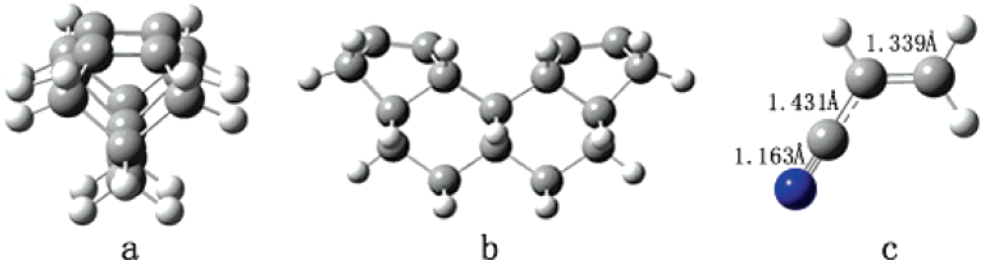

Figure 1. Optimized geometries of $C_{15}H_{16}$ and $C_{23}H_{24}$ clusters and free acrylonitrile molecule.

SCHEME 1: Schematic Diagrams for the Two Possible Reaction Pathways of Acrylonitrile with One Surface Dimer

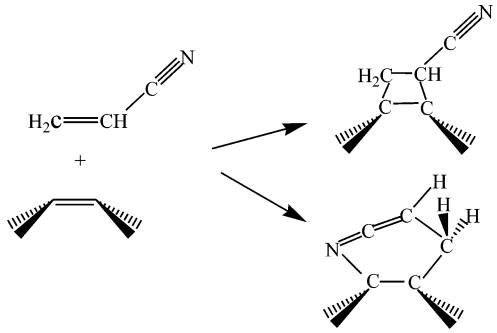

functional theory (DFT) calculations. Scheme 1 shows two possible reaction pathways of acrylonitrile with one surface dimer: [2+2] cycloaddition and [4+2] cycloaddition. Our results suggest that the chemisorption is a complex process, which can undergo both [4+2] and [2+2] cycloaddition reactions, involving not only single C dimer units but also the neighboring C═C dimers along and across the dimer rows. We find that the reaction of acrylonitrile with the diamond (001) surface occurs primarily through its nonpolar C═C group and the intradimer $[2+2]_{cc}$ product is the dominant product. These results are in good agreement with the experimental work by Schwartz et al.[22]

2. Computational Details

Surface structures with interfacial bonding involving more than one surface dimer may also exist. Hovis et al.[26] and Lu et al.[27] have reported interdimer surface structures on Si(100) surface. So it inspires us with the possibility that interdimer adsorption may also occur on the diamond (001) surface. Here, in our quantum chemical calculations, two cluster models were employed. First, a $C_{15}H_{16}$ cluster model was employed to represent two neighboring C═C dimers within the same row of the C(001)-2×1 surface. This cluster model consists of four layers of atoms, with four C atoms in the top layer comprising the surface dimers, six second-layer diamond atoms, three third-layer diamond atoms, and two fourth-layer diamond atoms. To study the interrow reactions, another model, a $C_{23}H_{24}$ cluster model, was adopted (Figure 1b). This cluster model consists of five layers of atoms, with four C atoms in the top layer comprising the surface dimers, eight second-layer diamond atoms, six third-layer diamond atoms, three fourth-layer diamond atoms, and two fifth-layer diamond atoms. Since cluster models are used, it is clear that the predicted reaction mechanism only limits to the case at low surface coverage. At higher surface coverage, there will be a clear steric repulsion. If clusters are properly selected, the cluster models can present advantages in terms of a compromise between accuracy and computational cost. All calculations were performed with the help of Gaussian 03[28] programs on ShuGuang4000A workstations in Ludong University. The standard 6-31G* basis set and the hybrid density functional theory (B3LYP) method, including Becke's three-parameter non-local-exchange functional[29] with the correlation functional of Lee−Yang−Parr,[30] were used for geometry optimizations. Recent studies have consistently reinforced the reliability of using this theoretical method to study surface reactions on the diamond surfaces.[16,18−21,31−33] Geometry optimizations with no constrained degrees of freedom were carried out by use of analytical gradients and the Berny algorithm.[34] To follow the minimum energy path (MEP), detailed intrinsic reaction coordinate (IRC) calculations were performed. Reported energies have not been corrected with zero-point energy (ZPE), unless otherwise specified. The optimized geometries of the $C_{15}H_{16}$ and $C_{23}H_{24}$ clusters and free acrylonitrile are presented in Figure 1.

3. Results and Discussion

Eight unique reaction channels involving two surface dimers along and across the dimer rows were identified: (a) $[2+2]_{cc}$ intrachannel (reaction between the vinyl group and one surface dimer); (b) $[2+2]_{cc}$ interchannel (reaction between the vinyl group and two neighboring C═C dimers); (c) [4+2] intrachannel (forming a six-membered structure on one surface dimer); (d) [4+2] interchannel (forming a seven-membered structure on two dimers); (e) $[2+2]_{CN}$ channels; and (f) $[2+2]_{cc}$ and [4+2] reactions across rows. The resulting energetic data are presented in Table 1. The separated acrylonitrile and bare surface serve as the reference energy point (Re) for the other stationary points on the potential energy surface.

A. $[2+2]_{cc}$ Intrachannel. This $[2+2]_{cc}$-like cycloaddition is initiated by the vinyl group of acrylonitrile and one surface dimer. Optimized structures for this channel are presented in Figure 2.

First, our calculations predict that it can proceed through a low-symmetry pathway with an activation barrier of 45.77 kcal/mol. Figure 3 depicts the potential energy profile of this process. Since a [2+2] cycloaddition, in general, is symmetry-forbidden according to Woodward−Hoffmann rules, the symmetric path has a large barrier. However, the new bonds are formed asymmetrically via transition state TS1 to form Pro1 directly. As shown in Table 1, the intradimer $[2+2]_{cc}$ product Pro1 has an energy of −64.33 kcal/mol, which predicts that it is the most thermodynamically stable product formed on the $C_{15}H_{16}$ cluster. Since this channel has the highest activation barrier, it is not kinetically favorable. So the intradimer $[2+2]_{cc}$ reaction is unlikely to occur through this process, except at very high temperatures. In fact, our calculations suggest that the intradimer $[2+2]_{cc}$ product Pro1 should be formed by the isomerization of the intradimer [4+2] product that will be discussed later.

As shown in Figure 2A, an asymmetric transition state TS1 in this process was located. This transition state is responsible for a low-symmetry [2+2] pathway along the potential energy

TABLE 1: Relative Energies of Stationary Points along the Reaction Channels[a]

$[2+2]_{cc}$ intra		$[2+2]_{cc}$ inter		[4+2] intra		[4+2] inter		$[2+2]_{CN}$[b]		interrow[c]	
SP[d]	RE[e]	SP	RE	SP	RE	SP	RE	SP	RE	SP	RE
TS1	45.77	TS2a	12.08	TS4	9.24	TS3a	9.04	LM5	28.33	TS7	10.84
TS1a	9.84	LM2	11.82	Pro4	−34.27	LM3	8.82	LM6	28.38	LM7	−13.77
LM1	9.63	TS2b	15.26	TS4a	3.90	TS3b	15.40	TS5	9.90	TS8	−8.04
TS1b	10.82	TS2c	9.66	LM4	−28.82	Pro3	−15.45	TS6	9.72	TS9	18.78
Pro1	−64.33	Pro2	−37.78	TS4b	8.67					Pro5	−69.58
										Pro6	−10.73

[a] Values are energies relative to separated reactants and are given in kilocalories per mole. [b] $[2+2]_{CN}$ channels, [c] Interrow reactions, [d] Stationary points, [e] Relative energies.

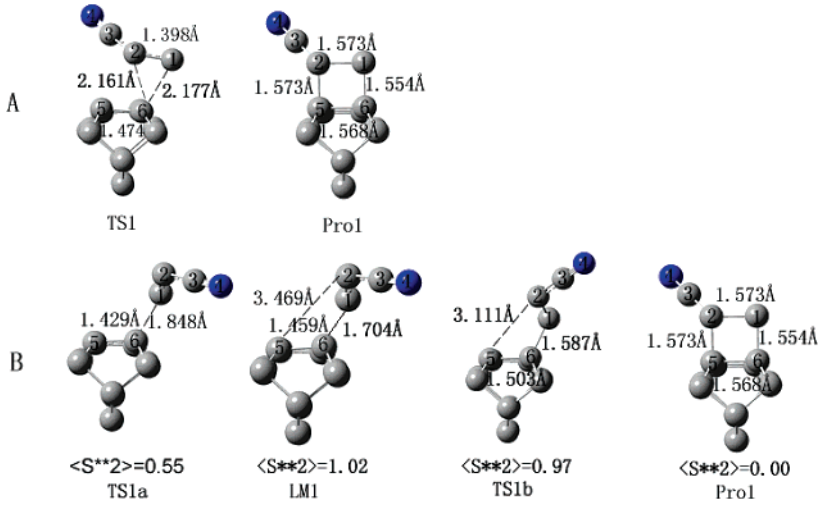

Figure 2. Optimized structures for $[2+2]_{cc}$ intrachannel (hydrogens are not shown). $\langle S^2 \rangle$ values for the wave functions of some stationary points are also given.

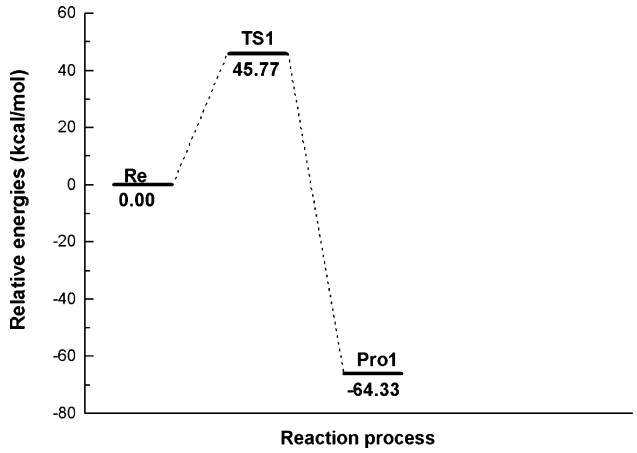

Figure 3. Potential energy profile of intradimer $[2+2]_{cc}$ reaction.

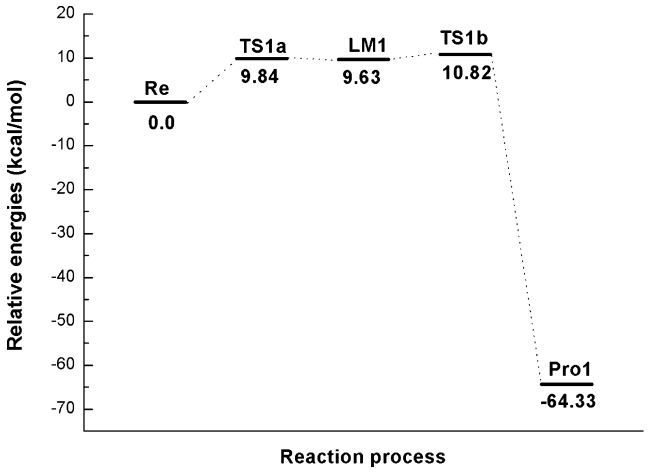

Figure 4. Potential energy profile of the intradimer $[2+2]_{cc}$ reaction occurring via stepwise mechanism.

surface of the closed-shell singlet electronic state. In this transition state, a three-membered ring is formed between the vinyl group and the C6 atom of the surface dimer. The distances of C1−C6 and C2−C6 are 2.177 and 2.161 Å, respectively. It is noteworthy that the C2−C6 bond length is the shortest distance between the two reactants. In Pro1, the two newly formed C1−C6 and C2−C5 bond lengths are 1.554 and 1.573 Å, respectively. The dimer bond increases from 1.359 Å before reaction to 1.568 Å, consistent with a bond order change from double to single. The reacting acrylonitrile double-bond length changes similarly.

C(001) surface dimers have been predicted to have biradicaloid character,[35] and the theoretical calculations show that [2+2] reactions between butadiene or ethylene and C(001) surface are facilitated by a diradical intermediate.[32,33] So the intradimer $[2+2]_{cc}$ reaction may also proceed through a two-step process via a diradical intermediate. In fact, our calculations suggest that the intradimer $[2+2]_{cc}$ reaction can also proceed through a two-step process (Figure 2B). The mechanism of this process is similar to those reported by Fitzgerald and Doren[32] and Lu et al.[36] Figure 4 depicts the potential energy profile of this process. The diradical species along this reaction pathway require unrestricted wave functions in the DFT calculations. The first kinetic barrier is the transition state TS1a to formation of one C−C bond with the surface, calculated to be 9.84 kcal/mol with respect to the reactants. The length of the nascent C1−C6 bond is 1.848 Å at this point. An intermediate LM1 with an energy of 9.63 kcal/mol with respect to the reactants was located. Spin density analysis on the wave functions of LM1 reveals that the unreacted C2 and C5 atoms have spin densities of −0.83

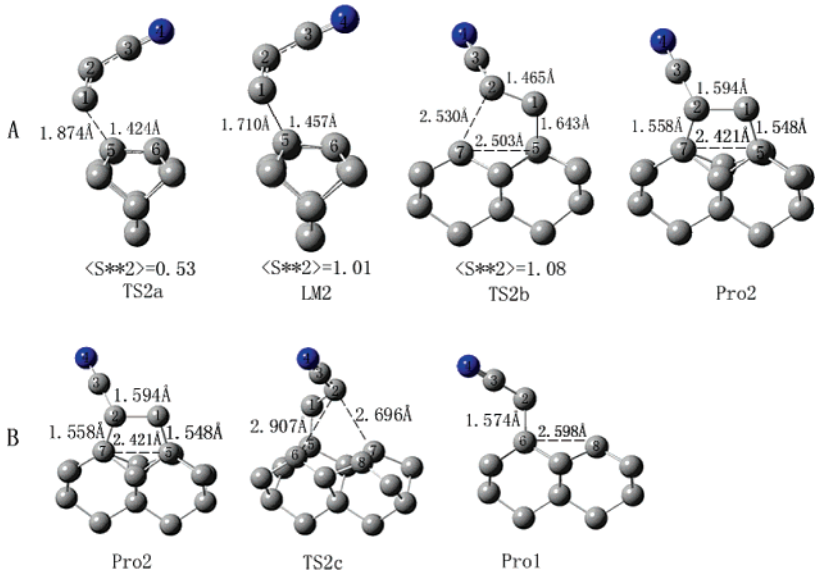

Figure 5. Optimized structures for $[2+2]_{cc}$ interchannel (hydrogens are not shown). (A) Process for formation of Pro2; (B) isomerization of Pro2.

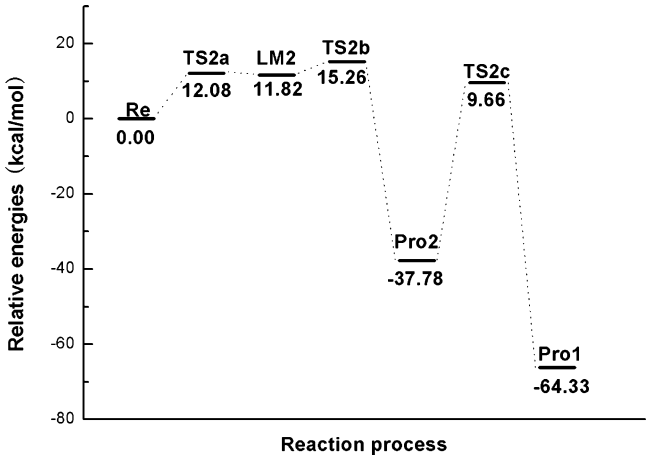

Figure 6. Potential energy profile of interdimer $[2+2]_{cc}$ reaction at the level of UB3LYP/6-31G*.

and +0.92, respectively, indicating that the two unpaired electrons are mainly localized on these two carbon atoms. From LM1, the intradimer $[2+2]_{cc}$ product Pro1 can be formed by overcoming a barrier of 10.82 kcal/mol at the transition state TS1b. The forming C2−C5 bond length is 3.111 Å at this point. It is noteworthy that TS1b is a rotational transition state. In TS1b, the length of C1−C6 is 1.587 Å, while the dihedral angle of $-C_6C_1C_2C_3$ is increased to 135.29°, compared with the value of 91.40° in LM1. The −CN group is vibrating in the direction of increasing the dihedral angle of $-C_6C_1C_2C_3$. With the reaction going on, the −CN group rotated from outside to inside and formed the final product Pro1 with the value of the dihedral angle of $-C_6C_1C_2C_3$ been changed from 91.40° (in LM1) to −126.11° (in Pro1). In this process, the formation of TS1b is the rate-determining step. Compared with the one-step mechanism, the two-step process is much more favorable.

B. $[2+2]_{cc}$ Interchannel. In fact, our calculations suggest that the interdimer $[2+2]_{cc}$ adsorption can also occur. This interdimer $[2+2]_{cc}$ reaction involving two surface dimers within the same row proceeds through a two-step process (Figure 5A). Figure 6 depicts the potential energy profile of this process. As shown in Figure 5A, the first kinetic barrier is the transition state TS2a, calculated to be 12.08 kcal/mol above the reactants. The length of the forming C1−C5 bond is 1.874 Å at this point, which is shortened to 1.710 Å in the intermediate LM2. LM2 has an energy of 11.82 kcal/mol with respect to the reactants. Spin-density analysis on the wave functions of LM1 reveals that the unreacted C2 and C6 atoms have spin densities of −0.93 and +0.80, respectively, indicating that the two unpaired electrons are mainly localized on these two carbon atoms. From the singlet-diradical intermediate LM2, interdimer $[2+2]_{cc}$ adsorption can occur through a transition state TS2b, leading to the formation of the interdimer $[2+2]_{cc}$ product Pro2. TS2b is 15.26 kcal/mol above the reactants. The forming C2−C7 bond length is 2.530 Å at this point. Such an interdimer process with a predicted exothermicity of 37.78 kcal/mol appears to be less exothermic than the intradimer $[2+2]_{cc}$ cycloaddition, probably due to the presence of two radicallike dangling bonds at the unreacted ends of two neighboring surface dimers. Though it is not as stable as Pro1, it is still an important thermodynamic structure.

As shown in Figure 5A, in the five-membered product Pro2, the two newly formed C1−C5 and C2−C7 bond lengths are 1.548 and 1.558 Å, respectively. Compared with the value of 1.339 Å in free acrylonitrile, the distance between C1 and C2 is increased to 1.594 Å, indicating the conversion from C1═C2 double bond to C1−C2 single bond upon chemisorption. It is noteworthy that the C5−C7 distance is shortened to 2.421 Å, compared with the value of 2.602 Å in reactant.

More importantly, the interdimer $[2+2]_{cc}$ product Pro2 can isomerize to the intradimer $[2+2]_{cc}$ product Pro1. The transition state TS2c is reached by breaking the C2−C7 bond and forming the C2−C6 bond. This transition state connects final products Pro1 and Pro2 with an activation barrier of 9.66 kcal/mol relative to the separated reactants. The cleaving C2−C7 bond length and the forming C2−C6 bond length at this point are 2.696 and 2.907 Å, respectively (Figure 5B). In the final product Pro1, the distances of C6−C8 and C5−C7 are 2.598 and 2.600 Å, respectively. So, compared with the value of 2.602 Å in reactant, they have little change. This isomerization process predicts that the residual π-character in the initially adsorbed species can be used for surface isomerizations. In this process, the formation of TS2b is the rate-determining step. If the interdimer product Pro2 is formed, then the intradimer product Pro1 can be formed readily.

C. [4+2] Intrachannel. This channel, which involves conjugated C═C/C≡N and one surface dimer, gives rise to a six-membered adduct Pro4. Figure 7 depicts the potential energy

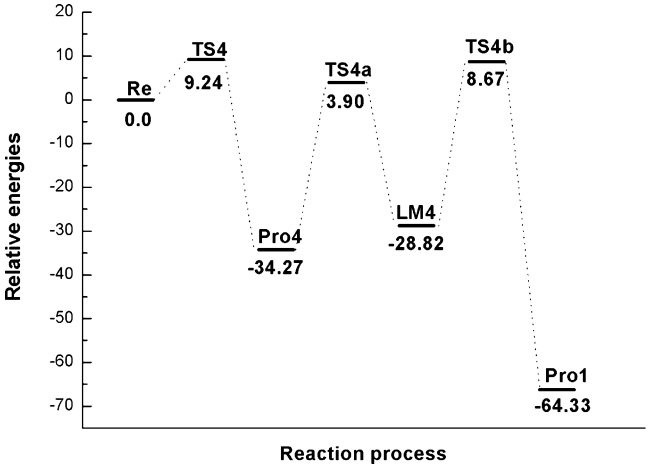

Figure 7. Potential energy profile of intradimer [4+2] reaction at the level of UB3LYP/6-31G*.

profile of this channel. Pro4 has a stabilization energy of −34.27 kcal/mol relative to the separated reactants. So, although Pro4 is less stable than Pro1 and Pro2, it appears to be thermodynamically important.

This channel is concerted with an asymmetric transition state TS4 (Figure 8A). The activation barrier is 9.24 kcal/mol above the separated reactants. This is the only transition state found, though searches for the second transition state were attempted. IRC calculations demonstrate that it is a concerted mechanism. In TS4, the forming C1−C6 and C5−N4 bond lengths are 1.905 and 4.253 Å, respectively. The difference $\Delta d = 2.348$ Å is quite large, possibly due to the lone pair of electrons on the N4 atom. In Pro4, the dimer bond is elongated by 0.26 Å with respect to the unreacted C5−C6 bond length, showing its single-bond character; in contrast, the C2−C3 bond length is shortened to 1.320 Å, showing its double-bond nature; the two newly formed C1−C6 and C5−N4 bond lengths are 1.56 and 1.50 Å, respectively. Furthermore, compared with the value of 1.163 Å for C3−N4 in free acrylonitrile, the length of C3−N4 is elongated to 1.237 Å, consistent with a bond order change from triple to double.

More importantly, Pro4 is not the final product in this channel, since it can isomerize to the intradimer $[2+2]_{cc}$ product Pro1 through a two-step process (Figure 8A). The first kinetic barrier is the transition state TS4a, calculated to be 3.90 kcal/mol above the reactants. A five-membered structure (LM4) was formed by breaking the C5−N4 bond and forming the C5−C3 bond at transition state TS4a. In TS4a, the cleaving C5−N4 bond length and the forming C5−C3 bond length are 2.243 and 1.65 Å, respectively. LM4 has a stabilization energy of −28.82 kcal/mol. In LM4, the newly formed C5−C3 bond length is 1.48 Å; the C2−C3 and C3−N4 bond lengths are 1.443 and 1.267 Å, respectively. TS4b is the second transition state with an energy of 8.67 kcal/mol relative to the separated reactants. The cleaving C5−C3 bond length and the forming C5−C2 bond length at this point are 1.80 and 2.273 Å, respectively. Detailed geometry parameters can be found in the Supporting Information. The low energy barriers in this isomerization process suggest that the isomerization is important in the chemisorption process.

D. [4+2] Interchannel. This interdimer [4+2] reaction also proceeds through a two-step process. Figure 9 depicts the potential energy profile of this process. The first kinetic barrier is the transition state TS3a to form the C1−C5 bond, calculated to be 9.04 kcal/mol above the reactants. The forming C1−C5 bond length is 1.858 Å at this point. An intermediate LM3 with an energy of 8.82 kcal/mol was located (Figure 8B). The distance of C1−C5 is 1.714 Å at this point. TS3b is the second transition state with an energy of 15.40 kcal/mol. In this process, the formation of the TS3b is the rate-determining step. As shown in Table 1, Pro3 has a stabilization energy of −15.45 kcal/mol, which is the highest energy of all four products formed on the $C_{15}H_{16}$ cluster model.

In TS3b (Figure 8B), the forming C7−N4 bond length is 2.276 Å, which is shortened to 1.503 Å in the seven-membered product Pro3. In Pro3, the C2−C3 bond length is 1.315 Å, showing its double-bond character. The C3−N4 bond length increases from 1.163 to 1.233 Å, similar to that in Pro4. It is

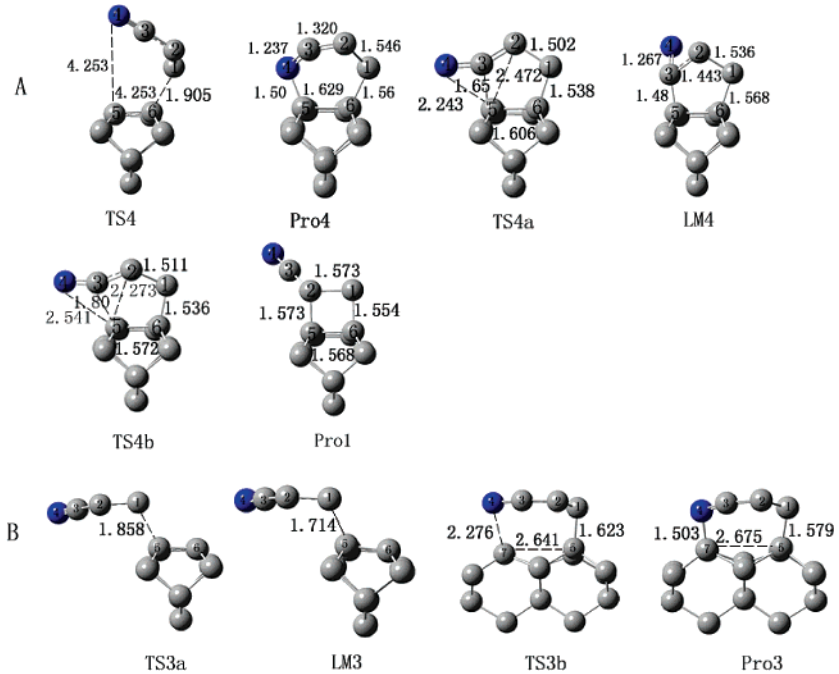

Figure 8. Optimized structures (units of angstroms for bond length) for [4+2] reactions: (A) [4+2] intradimer; (B) [4+2] interdimer same row (hydrogens are not shown).

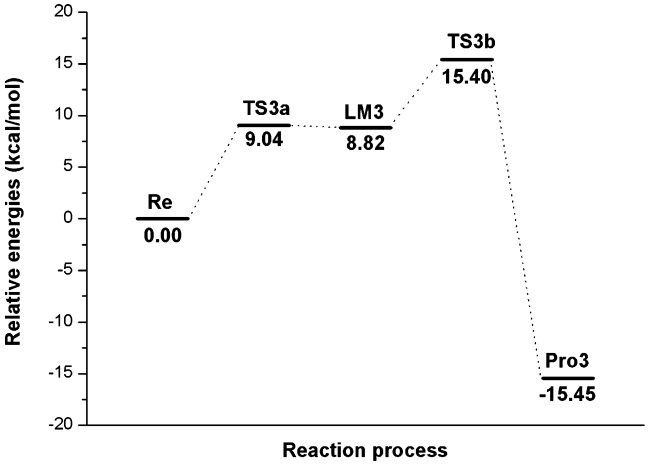

Figure 9. Potential energy profile of interdimer [4+2] reaction at the level of UB3LYP/6-31G*.

noteworthy that the C5−C7 distance is elongated to 2.675 Å, compared with the value of 2.602 Å in reactant.

E. $[2+2]_{CN}$ Channel. Except for the channels discussed above, the [2+2] cycloaddition of the cyanide group to the surface dimer may also occur. Two transition states (TS5 and TS6) were located. The two transition states lead to the formation of intradimer $[2+2]_{CN}$ product and interdimer $[2+2]_{CN}$ product, respectively (Figure 10). The energies of the two transition states are 9.90 and 9.72 kcal/mol, respectively. It is noteworthy that the two transition states are the last steps of the formation of the two $[2+2]_{CN}$ products. The first step of the intradimer $[2+2]_{CN}$ reaction results in the formation of the intermediate LM5, while the first step of the interdimer $[2+2]_{CN}$ reaction is the formation of the intermediate LM6 in which the N4 atom is bonded to the C6 atom. The relative energies of LM5 and LM6 are 28.33 and 28.38 kcal/mol, respectively. But the transition states between reactants and the two intermediates (LM5 and LM6) were not located. If they exist, their energies must be higher than that of LM5, so compared with the other channels, the two $[2+2]_{CN}$ pathways are not favorable.

F. $[2+2]_{cc}$ and [4+2] Interchannels across the Dimer Row. In fact, our calculations suggest that the interdimer $[2+2]_{cc}$ and [4+2] adsorption across the dimer row can also occur. To study these two channels, the $C_{23}H_{24}$ cluster model was employed. Optimized structures for these two channels are presented in Figure 11. The interdimer $[2+2]_{cc}$ reaction also proceeds through a two-step process. Figure 12 depicts the potential energy profile of this channel. The first kinetic barrier is the transition state TS7 to form the C1−C6 bond, calculated to be 10.84 kcal/mol above the reactants. The forming C1−C6 bond length is 1.888 Å at this point. An intermediate LM7 with an energy of −13.77 kcal/mol with respect to the reactants was located. The bond length of C1−C6 is 1.551 Å at this point, while the C2−C7 and N4−C7 distances are 4.117 and 4.713 Å, respectively. TS8 is the second transition state with an energy of −8.04 kcal/mol. The forming C2−C7 bond length is 2.854 Å at this point. In this process, the formation of the TS7 is the rate-determining step. Such an interdimer $[2+2]_{cc}$ process is predicted to be exothermic by 69.58 kcal/mol relative to isolated reactants. In

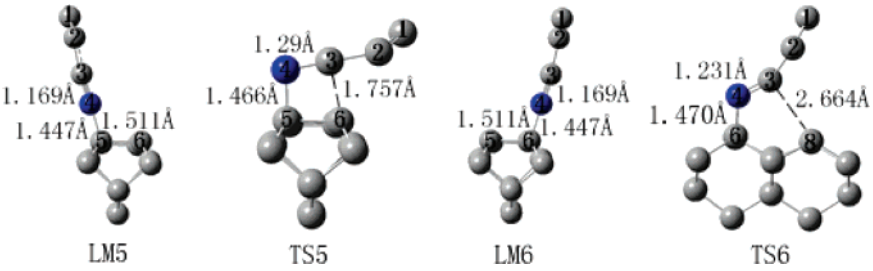

Figure 10. Optimized structures for $[2+2]_{CN}$ reactions (hydrogens are not shown).

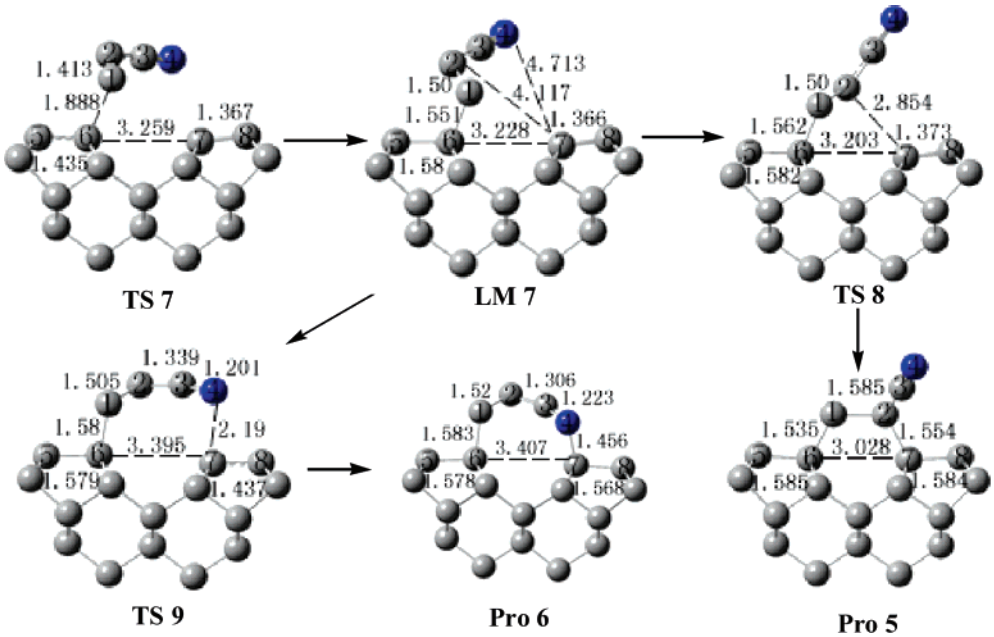

Figure 11. Optimized structures (units of angstroms for bond length) for interdimer $[2+2]_{cc}$ and [4+2] reactions across dimer row (hydrogens are not shown).

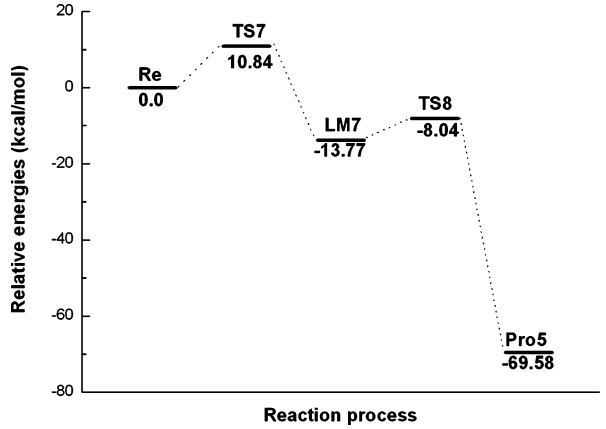

Figure 12. Potential energy profile of interdimer $[2+2]_{cc}$ reaction across the dimer row.

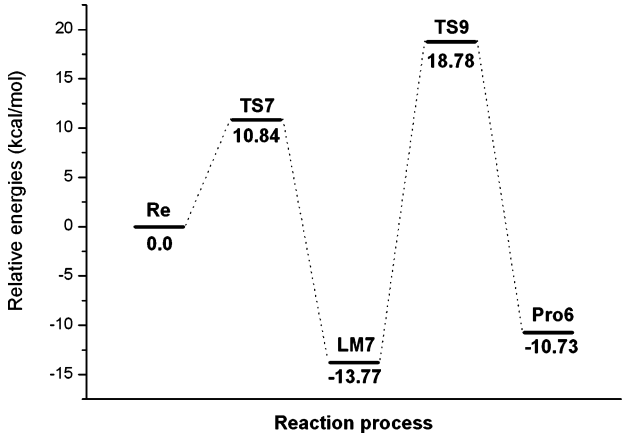

Figure 13. Potential energy profile of interdimer [2+2] reaction across the dimer row.

Pro5, the two newly formed C1−C6 and C2−C7 bond lengths are 1.535 and 1.554 Å, respectively; the C1−C2 distance increases from 1.339 Å before reaction to 1.585 Å, consistent with a bond order change from double to single. Furthermore, the C5−C6 and C7−C8 bond lengths are 1.585 and 1.584 Å, respectively, showing their single-bond nature.

As shown in Figure 11, from the intermediate LM7, interdimer [4+2] adsorption across the dimer row can also occur through a transition state TS9, leading to the formation of the interdimer [4+2] product Pro6. Figure 13 depicts the potential energy profile of this channel. TS9 is calculated to be 18.78 kcal/mol above the reactants. The forming N4−C7 bond length is 2.19 Å at this point. In this process, the formation of the TS9 is the rate-determining step. Such an interdimer [4+2] process is predicted to be exothermic by 10.73 kcal/mol relative to isolated reactants. In Pro6, the C2−C3 bond length is shortened to 1.306 Å, showing its double-bond nature; the two newly formed C1−C6 and N4−C7 bond lengths are 1.583 and 1.456 Å, respectively. Furthermore, compared with the value of 1.163 Å for C3−N4 in free acrylonitrile, the length of C3−N4 is elongated to 1.223 Å, consistent with a bond order change from triple to double.

G. Electronic Structures. Based on the above discussion, the [4+2] intrachannel is the main reaction channel and the [2+2] intrachannel is the second favorable channel, and the intradimer $[2+2]_{cc}$ product is the dominant product. Thus, we only discuss these two channels in this section.

These reactions appear to be under frontier molecular orbital (FMO) control, as the FMO model is capable of explaining the

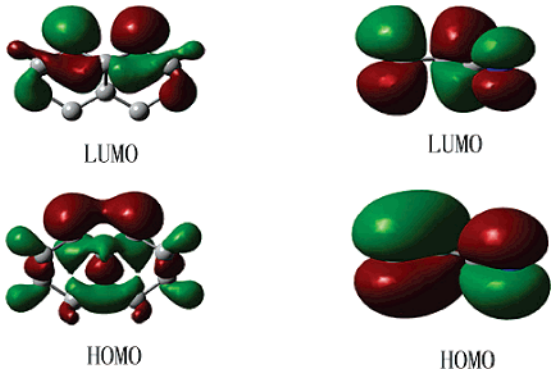

Figure 14. Frontier molecular orbitals of the diamond surface and acrylonitrile.

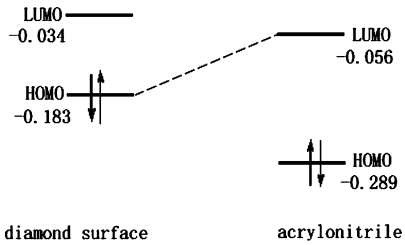

Figure 15. Interaction of frontier molecular orbitals on the reaction of acrylonitrile on C(001)-2×1 surface (orbital energies in hartrees).

effects of substituted groups for these inverse-electron-demand cycloadditions, which require an electron-poor diene and an electron-rich dienophile. Very recently, an analysis[37] based on the reactivity indexes defined within the DFT has been used to explain the reactivity of electron-deficient dienes and electron-deficient ethylenes in cycloaddition reactions. Recently, our group reported that Diels−Alder reactions of *o*-quinone methides and various substituted ethenes and found that the gap between the highest occupied and lowest unoccupied molecular orbitals (HOMO and LUMO) of two reactants is important to predict the reaction activity.[38]

Figure 14 shows the frontier molecular orbitals of the diamond surface and acrylonitrile, and Figure 15 gives their orbital energies. According to qualitative thoughts with orbital interaction theory, the interaction of two centers of a donor and one center of an acceptor is a peculiar feature of the initial stage of thermal [2+2] cycloaddition reactions between the electron donors and electron acceptors, which favors the interactions between the HOMO of the donor and the LUMO of the acceptor to the greatest extent.[39] It is obvious that the energy difference between $HOMO_{acry}$ and $LUMO_{diam}$ is greater than the difference of $HOMO_{diam}$ and $LUMO_{acry}$. Thus, the main HOMO−LUMO interaction occurs between $HOMO_{diam}$ and $LUMO_{acry}$, which indicates that the charge was transferred from diamond surface to acrylonitrile in the reaction process.

In fact, on the basis of the symmetry-adapted interaction of molecular orbital theory, the HOMO (d) of the C═C bond of diamond (the donor, denoted by D) is allowed by the orbital symmetry to interact with not only the LUMO (a*) but also the HOMO (a) of the C═C bond of acrylonitrile (an acceptor, denoted by A) (Scheme 2). The d−a* interaction results a charge transferred from d to a* orbital. In this process, a singlet diradical intermediate was formed. Theoretically, Lu et al.[40] first demonstrated that the adsorption of ethylene on Si(001)-2×1 surface follows a diradical mechanism. Similarly, Ma et al.[41] reported that all the transitions and intermediates have diradical character to different extents in the cycloaddition reaction of ethylene derivatives with Si(001)-2×1 surface. For the d−a*

SCHEME 2

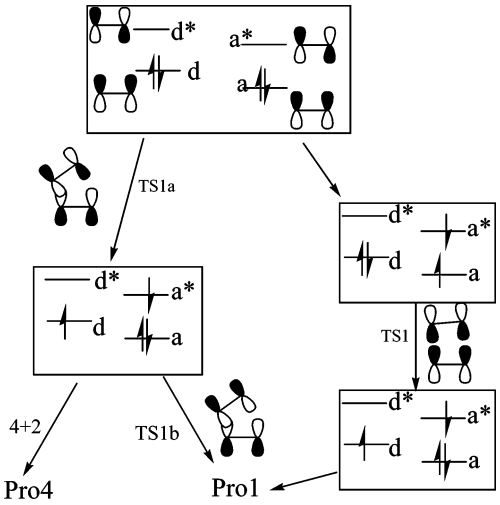

interaction, because there is a low energy gap between d and a*, the electron transfer from d to a* orbital is easy, and so the energy barrier of transition state TS1a is low, and this reaction take a singlet diradical mechanism. For interaction of HOMO (d) of the C═C bond of diamond with HOMO (a) of the C═C bond of acrylonitrile, it is first necessary that there is a electron shifting from HOMO (a) of the C═C bond of acrylonitrile to the LUMO (a*) of the C═C bond of acrylonitrile; then the d and a orbitals interacted with each other. In this process, the cycloaddition reaction is one-step and concerted. However, because of large energy gap between a and a* orbitals, the electron transfer from a to a* orbital is difficult, and so the energy barrier of TS1 is high (45.77 kcal/mol).

4. Conclusions

We have shown detailed reaction pathways for both [2+2] and [4+2] cycloaddition of acrylonitrile with the C(001)-2×1 surface. The calculations revealed eight possible reaction pathways for acrylonitrile with the surface dimer. Our results indicate that the reaction of acrylonitrile with the diamond (001) surface occurs primarily through its nonpolar C═C group and the intradimer $[2+2]_{cc}$ product is the dominant product. All these results are in good agreement with the experimental work by Schwartz. It is noteworthy that both the interdimer $[2+2]_{cc}$ product and the intradimer [4+2] product can isomerize to the intradimer $[2+2]_{cc}$ product. So the isomerization process plays an important role in the chemisorption process. The present study shows that the isomerization between intradimer [4+2] product and intradimer $[2+2]_{cc}$ product is slightly favorable over the direct path to formation of the intradimer $[2+2]_{cc}$ product. The formation of the intradimer [4+2] product is an important step for the formation of intradimer $[2+2]_{cc}$ product.

Acknowledgment. The support of the Natural Science Foundation of China (10404030) is gratefully acknowledged.

Supporting Information Available: Cartesian coordinates of all transition states and intermediates. This material is available free of charge via the Internet at http://pubs.acs.org.

References and Notes

(1) Ashfold, M. N. R.; May, P. W.; Rego, C. A.; Everitt, N. M. *Chem. Soc. Rev.* **1994**, *23*, 21.

(2) Hossain, Z.; Kubo, T.; Aruga, T.: Takag, N.; Tsuno, T.; Fujimori, N.; Nishijima, M. *Jpn. J. Appl. Phys.* **1999**, *38*, 6659.

(3) (a) *ThePproperties of Natural and Synthetic Diamond*; Field, J. E., Ed.; Academic Press: London, 1992. (b) *Diamond Films Handbook*; Asmussen, J., Reinhard, D. K., Eds.; Marcel Dekker: New York, 2002.

(4) Wei, J.; Yates, J. T., Jr. *Crit. Rev. Surf. Chem.* **1995**, *5*, 1.

(5) Grot, S. A.; Gisdenblat, G. Sh.; Hatfield, C. W.; Wronski, A. R.; Badzian, A. R.; Messier, T. R. *IEEE Elect. Dev. Lett.* **1990**, *11*, 100.

(6) Nakahata, H.; Imai, T.; Fujimori, N. *Diamond Materials*; Proceedings of the Electrochemical Society; , Pennington, NJ, 1991; Vol. 91−8, p 487.

(7) Pickett, W. E. *Phys. Rev. Lett.* **1994**, *73*, 1929.

(8) Van der Weide, J.; Nemanich, R. J. *J. Vac. Sci. Technol., B* **1994**, *12*, 2475.

(9) Malta, D. P.; Posthill, J. B.; Humphreys, T. P.; Thomas, R. E.; Fountain, G. G.; Rudder, R. A.; Hudson, G. C.; Mantini, M. J.; Markunas, R. J. *Appl. Phys. Lett.* **1994**, *64*, 1664.

(10) Mackey, B. L.; Russell, J. N., Jr.; Crowell, J. E.; Butler, J. E. *Phys. Rev. B* **1995**, *52*, 17009.

(11) Corkill, J. L.; Cohen, M. L. *Phys. Rev. B* **1993**, *48*, 7622.

(12) Liu, A. Y.; Cohen, M. L. *Science* **1989**, *245*, 841.

(13) Hovis, J. S.; Coulter, S. K.; Hamers, R. J. *J. Am. Chem. Soc.* **2000**, *122*, 732.

(14) Lu, X.; Xu, X.; Wang, N.; Zhang, Q. *J. Org. Chem.* **2002**, *67*, 515.

(15) Lu, X.; Xu, X.; Wang, N.; Zhang, Q. *J. Phys. Chem. B.* **2002**, *106*, 5972.

(16) Long, L. S.; Lu, X.; Tian, F.; Zhang, Q. *J. Org. Chem.* **2003**, *68*, 4495.

(17) Lu, X.; Fu, G.; Wang, N. Q.; Zhang, Q.; Lin, M. C. *Chem. Phys. Lett.* **2001**, *343*, 212.

(18) Xu, Y. J.; Zhang, Y. F.; Li, J. Q. *J. Org. Chem.* **2005**, *70*, 7773.

(19) Xu, Y. J.; Zhang, Y. F.; Li, J. Q. *J. Phys. Chem. B.* **2006**, *110*, 3197.

(20) Xu, Y. J.; Zhang, Y. F.; Li, J. Q. *J. Phys. Chem. B.* **2006**, *110*, 6148.

(21) Xu, Y. J.; Zhang, Y. F.; Li, J. Q. *J. Phys. Chem. B.* **2006**, *110*, 13931.

(22) Schwartz, M. P.; Barlow, D. E.; Russell, J. N., Jr.; Butler, J. E.; D'Evelyn, M. P.; Hamers, R. J. *J. Am. Chem. Soc.* **2005**, *127*, 8348.

(23) Furthmuller, J.; Hafner, J.; Kresse, G. *Phys. Rev. B.* **1996**, *53*, 7334.

(24) Yang, C.; Kang, H. C. *J. Chem. Phys.* **1999**, *110*, 11029.

(25) (a) Weiner, B.; Skokov, S.; Frenklach, M. *J. Chem. Phys.* **1995**, *102*, 5486. (b) Yang, C.; Kang, H. C. *Surf. Sci.* **1998**, *409*, 521.

(26) Hovis, J. S.; Hamers, R. J. *J. Phys. Chem. B.* **1998**, *102*, 687.

(27) Lu, X.; Zhu, M. P. *Chem. Phys. Lett.* **2004**, *393*, 124.

(28) Frisch, M. J.; Trucks, G. W.; Schlegel, H. B.; Scuseria, G. E.; Robb, M. A.; Cheeseman, J. R.; Montgomery, J. A., Jr.; Vreven, T.; Kudin, K. Mennucci, B.; Cossi, M.; Scalmani, G.; Rega, N.; Petersson, G. A.; Nakatsuji, H.; Hada, M.; Ehara, M.; Toyota, K.; Fukuda, R.; Hasegawa, J.; Ishida, M.; Nakajima, T.; Honda, Y.; Kitao, O.; Nakai, H.; Klene, M.; Li, X.; Knox, J. E.; Hratchian, H. P.; Cross, J. B.; Adamo, C.; Jaramillo, J.; Gomperts, R.; Stratmann, R. E.; Yazyev, O.; Austin, A. J.; Cammi, R.; Pomelli, C.; Ochterski, J. W.; Ayala, P. Y.; Morokuma, K.; Voth, G. A.; Salvador, P.; Dannenberg, J. J.; Zakrzewski, V. G.; Dapprich, S.; Daniels, A. D.; Strain, M. C.; Farkas, O.; Malick, D. K.; Rabuck, A. D.; Raghavachari, K.: Foresman, J. B.; Ortz, J. V.; Cui, Q.; Baboul, A. F.; Clifford, S.; Cioslowski, J.; Stefanov, B. B.; Liu, G.; Liashenko, A.; Piskorz, P.; Komaromi, I.; Martin, R. L.; Fox, D. J.; Keith, T.; Al-Laham, M. A.; Peng, C. Y.; Nanyakkara, A.; Challacombe, M.; Gill, P. M. W.; Johnson, B.; Chen, W.; Wong, M. W.; Gonzalez, C.; Pople, J. A. Gaussian03, Revision B.03; Gaussian, Inc.: Pittsburgh, PA, 2003.

(29) Becke, A. D. *J. Chem. Phys.***1993**, *98*, 5648.

(30) Lee, C.; Yang, W.; Parr, R. G. *Phys. Rev. B.*: *Condens. Matter* **1988**, *37*, 785.

(31) Okamoto, Y. *J. Phys. Chem. B* **2001**, *105*, 181.

(32) Fitzgerald, D. R.; Doren, D. J. *J. Am. Chem. Soc.* **2000**, *122*, 12334.

(33) Xu, Y. J.; Zhang, Y. F.; Li, J. Q. *J. Org. Chem.* **2005**, *70*, 6089.

(34) (a) Schlegel, H. B. *J. Comput. Chem.* **1982**, *3*, 214. (b) Schlegel, H. B. *Geometry Optimization on Potential Energy Surface in Modern Electronic Structure Theory*; Yarkony, D. R., Ed.; World Scientific Publishing: Singapore, 1994.

(35) Weiner, B.; Skokov, S.; Frenklach, M. *J. Chem. Phys.* **1995**, *102*, 5486.

(36) Lu, X.; Zhu, M.; Wang, X. *J. Phys. Chem. B* **2004**, *108*, 7359.

(37) (a) Sue, K.; Evanseck, J. D. *J. Am. Chem. Soc.* **2000**, *122*, 10418. (b) Domingo, L. R.; Arno, M.; Andres, J. *J. Org. Chem.* **1999**, *64*, 5867.

(38) Wang, H. M.; Wang, Y.; Han, K. L.; Peng, X. Q. *J. Org. Chem.* **2005**, *70*, 4910.

(39) (a) Inagaki, S.; Yamabe, S.; Fujimoto, H.; Fukui, K. *Bull. Chem. Soc. Jpn.* **1972**, *45*, 3510. (b) Inagaki, S.; Fukui, L. *Bull. Chem. Soc. Jpn.* **1973**, *46*, 2240. (c) Inagaki, S.; Minato, T.; Yamabe, S.; Fujimoto, H.; Fukui, K. *Tetrahedron* **1974**, *30*, 2165. (d) Inagaki, S.; Fukui, K. *J. Am. Chem. Soc.* **1975**, *97*, 7480.

(40) Lu, X.; Xu, X.; Wang, N.; Zhang, Q. *J. Am. Chem. Soc.* **2003**, *125*, 6834.

(41) Ma, J.; Wang, Y.; Inagaki, S.; Pei, Y. *J. Phys. Chem. B.* **2005**, *109*, 5199.